

Hybrid functional with semi-empirical van der Waals study of native defects in hexagonal BN

V. Wang,^{1,*} R.-J. Liu,¹ H.-P. He,² C.-M. Yang,¹ and L. Ma¹

¹*Department of Applied Physics, Xi'an University of Technology, Xi'an 710054, China*

²*Department of Geological Engineering, Lanzhou Resources & Environment Voc-Tech College, Lanzhou 730021, China*

(Dated: October 29, 2018)

ABSTRACT

The formation energies and transition energy levels of native defects in hexagonal BN have been studied by first-principles calculations based on hybrid density functional theory (DFT) together with an empirical dispersion correction of Grimme's DFT-D2 method. Our calculated results predict that the interstitial B is the most stable defect under N-rich and *p*-type conditions. While the B vacancy and interstitial N become the dominate defects when the electron chemical potential is near the conduction band maximum of host. Nevertheless, these compensating defects will be inactive due to their ultra deep ionization levels under both both *p*- and *n*-type conditions.

I. INTRODUCTION

Boron nitride exists in various phases, including cubic (*c*-BN), wurtzite (*w*-BN), hexagonal (*h*-BN) structures. Similar to graphite, *h*-BN consists of stacked BN layers with equal numbers of boron and nitrogen atoms. Within each *h*-BN layer, alternating boron and nitrogen atoms form a honeycomb sheet by *sp*²-hybridization; while the interlayer attractive force is mediated by weak van der Waals interactions. In contrast to the semimetallic behavior of graphite, *h*-BN is a wide band-gap semiconducting material due to its partially ionic character of B-N bond. Because it has high temperature stability, low dielectric constant, high mechanical strength, large thermal conductivity, high hardness, and high corrosion resistance. It is a promising material for the realization of compact ultraviolet laser devices, high-temperature and high-pressure devices.¹⁻⁴ Furthermore, it can be well integrated with graphene to design new novel devices as they have small mismatch (1.6%) and the same hexagonal structure.^{5,6}

h-BN is commonly synthesized through mechanical,⁷ liquid-phase exfoliation,⁸ or chemical vapor deposition (CVD).⁹⁻¹² During the process of *h*-BN growth, native defects are thus readily formed in an uncontrolled way, and they can be unintentionally generated to modify the conductivity of *h*-BN. Recently, Shi *et al.* synthesized *h*-BN films with the thickness up to 20 μm on the Ni surface by CVD. They pointed that the B/N ratio reaches to be 1:1.12 detected by X-ray photoelectron spectroscopy.¹¹ Previous theoretical studies have investigated the native defects in *h*-BN based on traditional density functional theory (DFT) within generalized gradient approximation (GGA) or local density approximation (LDA).^{13,14} The native defect properties of *h*-BN bilayer and monolayer have also been studied in our earlier DFT-GGA calculations.¹⁵ However, the severe underestimation of traditional DFT on the band gap of semiconductors, especially in the wide-gap semiconductors, results in large uncertainties in the position of defect levels and the stability of defects.^{13,16-21} The recent develop-

ment of hybrid density functional theory,²² which mix a fraction of Hartree-Fock (HF) exchange with the LDA or GGA exchange and correlation potentials, can correct the band gap²³ and provide more reliable description of transition levels and formation energies of defect in semiconductors.²⁴⁻²⁷

In this paper, we have systematically investigated the formation energies and transition energies of native defects in *h*-BN using hybrid density functional theory. We found that the calculated transition energies of all native defects are ultra deep and thus neither of them cannot contribute or compensate specific conductivity by extrinsic doping. The remainder of this paper is organized as follows. In Sec. II, the details of the computation are described. Sec. III presents our calculated formation energies and single particle energy levels of native defect in bulk hexagonal BN. Finally, a short summary is given in Sec. IV.

II. METHODS

Our total energy and electronic structure calculations were based on spin-polarized Kohn-Sham theory with the hybrid functional proposed by Heyd, Scuseria, and Ernzerhof (HSE)²², employing the projector augmented wave potentials³⁰ as implemented in the VASP code.^{28,29} In the HSE approach, a screening parameter of 0.2 \AA^{-1} was used as suggested for the HSE06 functional.³¹ We found that a proportion of $\alpha=33\%$ HF exchange with 67% GGA of Perdew, Burke and Ernzerhof (PBE)³² exchange produces an accurate value of the band gap for *h*-BN. The weak van der Waals interaction between layers plays a key role in determining the interlayer distance for layered materials. We incorporated the van der Waals interactions through employing an empirical correction scheme of Grimme's DFT-D2 method, which has been proven to be successful in describing the geometries of layered materials.^{33,34} *h*-BN has five possible structures. More details about the effects of stacking behavior can be found in Refs. 35 and 36. The most stable AB-like

stacking sequence with each boron atom on top of a nitrogen atom was adopted in our current study. The DFT-D2 (global scaling factor $s_6=0.40$) plus HSE06 ($\alpha=0.33$) scheme gives the calculated optimized lattice constants $a=2.50$ Å and $c=6.42$ Å, in good agreement with the experimental values of $a=2.50$ and $c=6.66$ Å respectively.³⁷

The defect systems were modeled by adding (removing) an atom to (from) in a $4\times4\times2$ supercell consisting of 128 atoms. The wave functions were expanded by plane waves up to a cutoff energy of 300 eV. The integrations over the Brillouin zone were performed using Γ -centered $2\times2\times2$ k-point mesh generated by Monkhorst-Pack scheme.³⁸ The internal coordinates in the defect supercells were relaxed to reduce the residual force to less than 0.02 eV·Å⁻¹. In the charged-defect calculations, a uniform background charge was added to keep the global charge neutrality of supercell. The formation energy of a charged defect was defined as³⁹

$$\Delta E_D^f(\alpha, q) = E_{tot}(\alpha, q) - E_{tot}(0) - \sum n_\alpha \mu_\alpha + q(\mu_e + \epsilon_v + \Delta V_{align}[q]), \quad (1)$$

where $E_{tot}(\alpha, q)$ and $E_{tot}(0)$ are the total energies of the supercells with and without defect α . n_α is the number of species α ($\alpha=B, N$) needed to create the defect α . μ_α is the corresponding atomic chemical potential, and q is the charge state of defect. μ_e is electron chemical potential in reference to the valence band maximum (VBM, denoted as ϵ_v) of bulk h -BN. Therefore, the electron chemical potential varies between zero and the band-gap E_g of host. The potential offset $\Delta V_{align}[q]$ is determined by the difference of the atomic-sphere-averaged electrostatic potentials around host atoms farther away the defect α , relative to the atomic-sphere-averaged electrostatic potentials around host atoms in the defect-free supercell.^{40,41}

The chemical potential μ_α depends on the experimental growth conditions. The chemical potentials of boron and nitrogen are subject to their lower bounds satisfied by the constraint $\mu_{BN}(bulk) = \mu_B + \mu_N$, where $\mu_{BN}(bulk)$ is the total energy of per formula unit of h -BN. The calculated formation energy of h -BN is -2.95 eV, slightly unstable 0.35 eV than the value obtained by the previous GGA-based calculation.¹³ The μ_N is subject to an upper bound given by the energy of one N atom (-10.34 eV) in a N₂ molecule, which corresponds to extreme N-rich/B-poor growth condition. Similarly, the upper bound of the μ_B is limited by the energy of one B atom (-7.65 eV) in boron bulk phase, corresponding to extreme B-rich/N-poor growth condition.

The transition-energy level $\epsilon_\alpha(q/q')$ of defect is the Fermi energy in Eq. (1) at which the formation energy $\Delta E_D^f(\alpha, q)$ of defect α with charge q is equal to that of another charge q' of the same defect. The $\epsilon_\alpha(q/q')$ can be calculated as

$$\epsilon_\alpha(q/q') = [\Delta E_D^f(\alpha, q) - \Delta E_D^f(\alpha, q')]/(q' - q). \quad (2)$$

III. RESULTS AND DISCUSSION

A. Pristine bulk h -BN

Despite the fact that there are a large number of experimental and theoretical studies on the bulk h -BN, its electronic properties are still a matter of debate: both direct and indirect band gap with the band gap values ranging from 3.20 to 5.97 eV have been reported. For example, Watanabe *et al.* showed that h -BN has an experimental direct band gap of 5.97 eV.¹ This result is in contradiction with the most recent quasiparticle theoretical calculations.^{42–44} Liu *et al.*³⁵ attributed such disagreement between experimental and theoretical reports to the coexistence of the sub-stable structures. Before proceeding to the results for the properties of native defects, it is worthwhile to investigate the band structure of h -BN. Our calculations show that the VBM situates at the H point, with the conduction band minimum (CBM) locating at the M point, as shown in Fig. 1(a). This leads to an indirect band gap of 5.92 eV, slightly smaller ~ 0.4 eV than the direct band gap at the H point. Analysis of the calculated partial density of state (PDOS) presented in Fig. 1(b), the upper valence band is dominated by N-2p states, with the lower conduction band comprising mostly of B-2p ones. In fact, as it will be shown in later, the highest occupied band (HOB) and the lowest unoccupied band (LUB) of bulk h -BN mainly derive from N-2p_z and B-2p_z respectively [see Fig. 2 (b)].

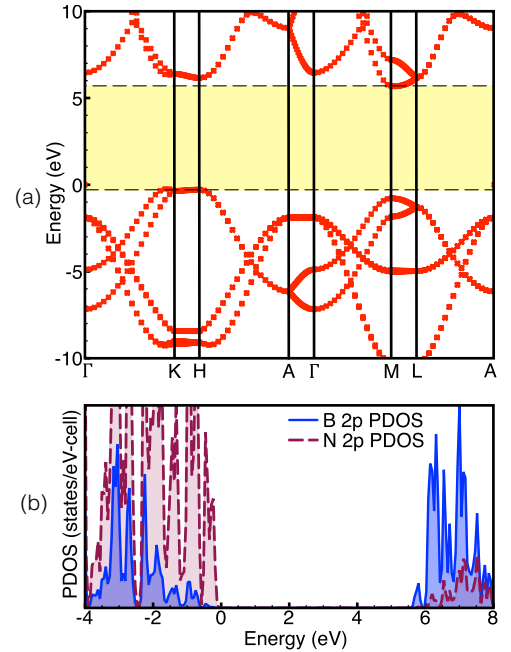


FIG. 1. (Color online) HSE06 calculated (a) band structure of h -BN, (b) N-2p and B-2p partial DOS in h -BN. The Fermi energy is set to zero.

B. Native defects in *h*-BN

In semiconductors and insulators, defects typically introduce levels in the band gaps of host materials. Therefore, we first examined the defect-induced DOS of the neutral B vacancy (V_B), N vacancy (V_N), interstitial B (B_i) and interstitial N (N_i), respectively. The calculated defect DOS are plotted in Fig. 2. In comparison with the DOS of defect-free system, one can note that the V_B introduces one (two) unoccupied defect level(s) in the spin-up (-down) component between around 2.6 and 3.6 eV above VBM. Thus it is expected that the possible charge states of V_B can vary from 0 to 3-. The V_N introduces one occupied defect state at $\epsilon_v+3.0$ eV in the spin-up component as well as one unoccupied level at $\epsilon_v+4.9$ eV in the spin-down component. Its possible charge states can range from 1+ to 1-. As shown in Fig. 2 (e), three occupied defects states and three unoccupied ones are introduced by the B_i . It should be pointed that the double-degenerate states occupied by four electrons just above CBM originate from the N- $2p_z$ states, instead of B_i . The reason is attributed to the interaction between the B_i and the N atoms in the adjacent BN layer. A wide range from 3+ to 3- can be expected for the possible charge states of B_i atom. Finally, we note that one occupied defect level at $\epsilon_v+0.1$ eV and one unoccupied level at $\epsilon_v+1.5$ eV are introduced by the N_i . Therefore, the 1+ charge state is the lowest achievable charges state for the N_i . Adding one, and two electrons into the unoccupied levels of N_i^{1+} results in the 0 and 1- charge states. Based on the results of defect induced DOS, one can find that the charge states of not all native defects can vary from 3+ to 3-.¹³ Nitrogen vacancy is a typical example.

For the neutral V_B , it is found that its wave functions localize symmetrically over all three N neighbors and show a sp^2 -like hybridized character [see Fig. 3 (a)]. No significant John-Teller distortion is observed, namely, the average N-N distances between these neighboring nitrogen atoms are almost equal to 2.7 Å. The N-N distances equably reduce to 2.6 Å when the V_B is in the charge state of 1-. It is close to the ideal N-N distance of 2.5 Å in perfect *h*-BN. We attribute the decrease of N-N distance to the repulsion between B atoms and the neighboring N ones of V_B . It is expected that N-N distances further reduce when V_B capture more extra electrons. On the other hand, in the case of V_B^{2-} , the strong Coulomb repulsion between the negatively charged N atoms results in the out-of-plane distortion for one (denoted as N_{out}) of them. Bader charge analysis⁴⁵ estimate that the N_{out} and the other two neighboring N atoms capture about 0.95 e and 0.44 e per N respectively due to the existence of symmetry breaking. Consequently, the N_{out} is observed to bind with the neighboring B atom in the adjacent BN layer, as shown in Fig. 3 (c). The V_B defect contributes 1 μ_B to the total magnetic moment of the system. Based on the defect levels induced by V_B , the total magnetic moments of the systems consisting of one V_B^{1-} , V_B^{2-} and V_B^{3-} are expected to be 2 μ_B , 1 μ_B and 0

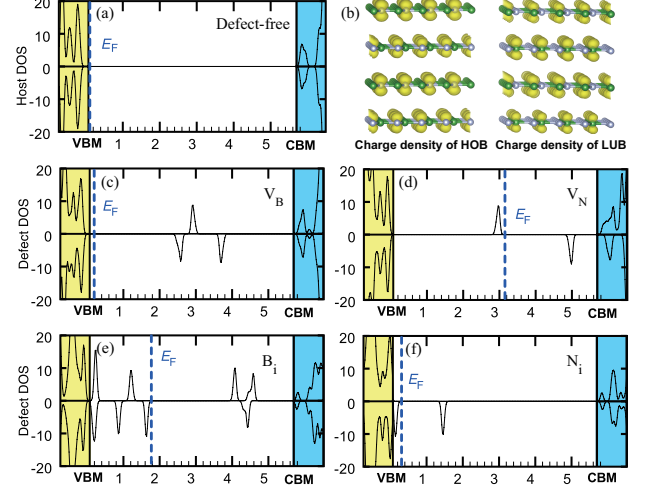


FIG. 2. (Color online) (a), (c), (d), (e) and (f) HSE06-calculated defect DOS for the bulk *h*-BN without native defect, with single neutral V_B , V_N , B_i and N_i respectively. Positive (negative) values refer to the spin-up (-down) component. The Fermi level is labeled by using a blue vertical line. (b) Band decomposed charge-density (isosurface: 0.001 e/bohr^3) for the highest occupied band (HOB) and the lowest unoccupied band (LUB) for the defect-free *h*-BN. Green and silver balls represent B and N atoms.

μ_B .

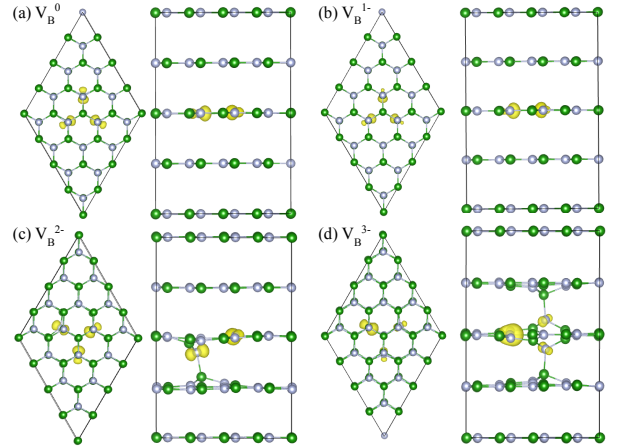


FIG. 3. (Color online) (a), (b), (c) and (d) Top and side views of the calculated charge-density for V_B in the charge state of neutral, 1-, 2- and 3-, respectively (isosurface: 0.05 e/bohr^3).

In contrast to the behavior of V_B , the wave functions of V_N defect states mainly localize on two of the three B neighbors and show a B- p_z character, as displayed in Fig.4. The B-B distances between these B neighbors relax inward from 2.4 Å for V_N^{1+} to 2.0 Å for V_N^{1-} . The changes of B-B distances almost undergo within the same BN layer plane when the V_N is in all possible charge

states, except for the 1- state. In the latter case, a slightly out-of-plane distortion is observed for the neighboring B atoms. As displayed in Fig. 2 (d), the occupied defect state at 3.0 eV above VBM leads to a magnetic moment of $1 \mu_B$ for the neutral V_N . As a result, both V_N^{1+} and V_N^{1-} have a local magnetic moment of $0 \mu_B$, according to the electron filling in these defect levels.

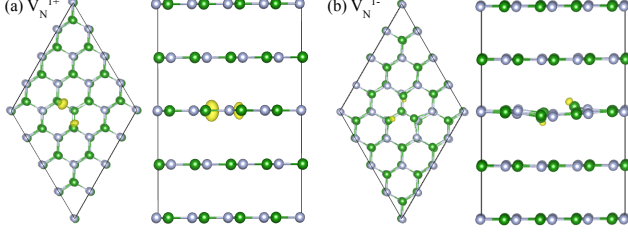


FIG. 4. (Color online) Top and side views of the calculated charge-density for the V_N defect-induced levels (isosurface: $0.05 e/\text{bohr}^3$). (a) V_N^{1+} , (b) V_N^{1-} .

There are three possible interstitial sites for B/N atom occupying in bulk h -BN. They are the hollow site above the center of a BN hexagon, the top site directly over a B atom, and the bridge site above the middle of a B-N bond. This is similar to the cases of transition-metal adsorbed on graphene layer or interstitial defects in the BN bilayer described in our previous studies.^{15,46} The optimized local structures of B_i under different charge states are more complicated than the native vacancies discussed above. As typical models, we display the relaxed local structures as well as the calculated band decomposed charge-density of B_i^{3+} and B_i^{3-} in Fig. 5 (a) and (b). We note that the B_i always favors the top site. It is found that a N-B- B_i -N vertical chain forms when the B_i in the $3+$ charge state. In contrast, the B_i^{3-} with its three B atoms neighbors binding tetrahedrally. The wave functions of defect levels are observed to mainly localize around the B_i atom. The magnetic moment of B_i in any possible charge state can be deduce from the calculated value of $1 \mu_B$ in the charge-neutral state.

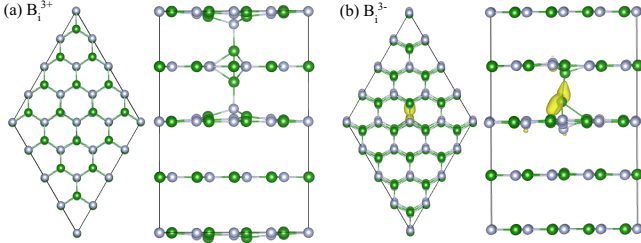


FIG. 5. (Color online) Top and side views of the calculated charge-density ($0.05 e/\text{bohr}^3$) for the B_i defect-induced levels (isosurface: $0.05 e/\text{bohr}^3$). (a) B_i^{3+} , (b) B_i^{3-} .

The N_i also favors the top site. Interestingly, it is found that the N_i relaxes from the ideal top site towards a lattice nitrogen atom, pushing it away from the above BN

layer to form a N-N dumbbell-like structure as displayed in Fig. 6. One can note that the wave functions of defect levels induced by N_i mainly distribute around this structure. Furthermore, the local structure of defect charge-density of N_i seems to insensitive to its charge state. The calculated magnetic moment of N_i in the charge states of $1+$, 0 , and $1-$ are $0 \mu_B$, $1 \mu_B$ and $2 \mu_B$, respectively.

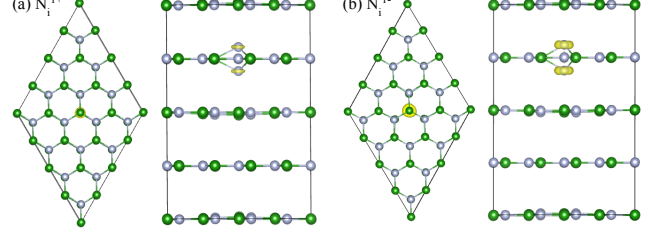


FIG. 6. (Color online) Top and side views of the calculated charge-density for the N_i defect-induced levels (isosurface: $0.05 e/\text{bohr}^3$). (a) N_i^{1+} , (b) N_i^{1-} .

Since the extreme B-rich growth condition which corresponds to very low nitrogen partial pressures is probably not experimentally accessible. In our present study, we only show the formation energies of native defects under N-rich growth condition. The formation energies of V_B , V_N , B_i and N_i defects as a function of electron chemical potential are plotted in Fig. 7. Under p -type condition when the E_F is near VBM, the B_i^{3+} with a formation energy of around -0.78 eV is found to be the most stable defect, in other words, its solubility is expected to be high under equilibrium growth conditions. The B_i can act as a donor-like defect, but its calculated transition level of $(3+/0)$ locates at 2.4 eV above VBM. This is a rather deep level, implying that it cannot compensate the p -type conductivity in h -BN. On the other hand, the formation energies of the other defects (V_B , V_N , and N_i) are high, at least 4.54 eV. This suggests that the concentration of these defect will be negligibly. When the electron chemical potential is close to CBM, the V_B and N_i become more stable with respect to the V_N and B_i . This is consistent with the experimental observation of higher concentration of nitrogen than that of boron.¹¹ The shallowest donor levels $(1-/2-)$ for N_i and $(2-/3-)$ for V_B occurs at 2.0 eV and 3.0 eV below CBM respectively. Thus, the dominating electron killers N_i and V_B are also ineffective under n -type conditions.

IV. SUMMARY

In summary, we have systematically studied the native defects in hexagonal BN using first-principles calculations based on hybrid density functional theory. The van der Waals interactions between BN layer were described via Grimme's DFT-D2 method. We first investigated the defect levels induced by the neutral native defects to determine the possible charge states of these

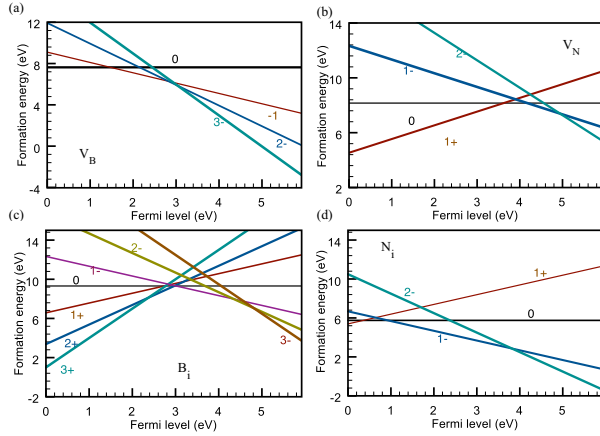


FIG. 7. (Color online) (a), (b), (c) and (d) The V_B , V_N , B_i and N_i formation energies as a function of the electron chemical potential under N-rich growth conditions respectively.

defects. Then we calculated the formation energies and local structures of various native defects as a function of

their possible charge states. We found that the B_i will dominate in h -BN under N-rich and p -type conditions. On the other hand, the V_B and N_i become more energetically stable when the electron chemical potential is near the conduction band maximum of host. The relaxed structures of native defects were found to be strongly dependent on their charge states. Finally, based on the calculated transition energies, Our results predicted that the energetically favorable defects will not act as effective charge compensating defects under both p - and n -type conditions due to their ionization levels are ultra deep.

ACKNOWLEDGMENTS

Wang acknowledges the support of the Natural National Science Foundation of Shaanxi Province (Grant No. 2013JQ1021) and the Doctoral Scientific Foundation of Xi'an University of Technology (Grant No. 108-211204). L. Ma acknowledges the support of the National Natural Science Foundation of China (Grant No. 51177133) and the Special Scientific Research Program of the Education Bureau of Shaanxi Province, China (Grant No. 2013JK1105).

-
- * Corresponding author at: Department of Applied Physics, Xi'an University of Technology, No.58, Yanxiang Road, Xi'an 710054, China, Tel./Fax: +86-29-8206-6357/6359 E-mail address: wangvei@icloud.com (V. Wang).
- ¹ K. Watanabe, T. Taniguchi, and H. Kanda, *Nat. Mater.* **3**, 404 (2004).
 - ² Y. Kubota, K. Watanabe, O. Tsuda, and T. Taniguchi, *Science* **317**, 932 (2007).
 - ³ K. Watanabe, T. Taniguchi, T. Niiyama, K. Miya, and M. Taniguchi, *Nat. Photonics* **3**, 591 (2009).
 - ⁴ J. Eichler and C. Lesniak, *J. Eur. Ceram. Soc.* **28**, 1105 (2008).
 - ⁵ C. Dean, A. Young, I. Meric, C. Lee, L. Wang, S. Sorgenfrei, K. Watanabe, T. Taniguchi, P. Kim, K. Shepard, *et al.*, *Nat. Nano.* **5**, 722 (2010).
 - ⁶ L. Britnell, R. V. Gorbachev, R. Jalil, B. D. Belle, F. Schedin, A. Mishchenko, T. Georgiou, M. I. Katsnelson, L. Eaves, S. V. Morozov, N. M. R. Peres, J. Leist, A. K. Geim, K. S. Novoselov, and L. A. Ponomarenko, *Science* **335**, 947 (2012).
 - ⁷ K. S. Novoselov, D. Jiang, F. Schedin, T. J. Booth, V. V. Khotkevich, S. V. Morozov, and A. K. Geim, *Proc. Natl. Acad. Sci. USA* **102**, 10451 (2005).
 - ⁸ J. N. Coleman, M. Lotya, A. O'Neill, S. D. Bergin, P. J. King, U. Khan, K. Young, A. Gaucher, S. De, and R. J. Smith, *Science* **331**, 568 (2011).
 - ⁹ C. Oshima and A. Nagashima, *J. Phys.: Condens. Matter* **9**, 1 (1997).
 - ¹⁰ M. Corso, W. Auwärter, M. Muntwiler, A. Tamai, T. Greber, and J. Osterwalder, *Science* **303**, 217 (2004).
 - ¹¹ Y. Shi, C. Hamsen, X. Jia, K. K. Kim, A. Reina, M. Hofmann, A. L. Hsu, K. Zhang, H. Li, Z.-Y. Juang, M. S. Dresselhaus, L.-J. Li, and J. Kong, *Nano Letters* **10**, 4134

- (2010).
- ¹² L. Song, L. Ci, H. Lu, P. B. Sorokin, C. Jin, J. Ni, A. G. Kvashnin, D. G. Kvashnin, J. Lou, B. I. Yakobson, and P. M. Ajayan, *Nano Letters* **10**, 3209 (2010).
- ¹³ W. Orellana and H. Chacham, *Phys. Rev. B* **63**, 125205 (2001).
- ¹⁴ Z.-L. Hou, M.-S. Cao, J. Yuan, X.-Y. Fang, and X.-L. Shi, *J. Appl. Phys.* **105**, 076103 (2009).
- ¹⁵ V. Wang, N. Ma, H. Mizuseki, and Y. Kawazoe, *Solid State Commun.* **152**, 816 (2012).
- ¹⁶ T. E. Mosuang and J. E. Lowther, *Phys. Rev. B* **66**, 014112 (2002).
- ¹⁷ A. Zobelli, C. P. Ewels, A. Gloter, and G. Seifert, *Phys. Rev. B* **75**, 094104 (2007).
- ¹⁸ S. Azevedo, J. R. Kaschny, C. M. C. de Castilho, and F. de Brito Mota, *Nanotechnology* **18**, 495707 (2007).
- ¹⁹ S. Okada, *Phys. Rev. B* **80**, 161404 (2009).
- ²⁰ L.-C. Yin, H.-M. Cheng, and R. Saito, *Phys. Rev. B* **81**, 153407 (2010).
- ²¹ N. Alem, O. V. Yazyev, C. Kisielowski, P. Denes, U. Dahmen, P. Hartel, M. Haider, M. Bischoff, B. Jiang, S. G. Louie, and A. Zettl, *Phys. Rev. Lett.* **106**, 126102 (2011).
- ²² J. Heyd, G. E. Scuseria, and M. Ernzerhof, *J. Chem. Phys.* **118**, 8207 (2003).
- ²³ M. Marsman, J. Paier, A. Stroppa, and G. Kresse, *J. Phys.: Condens. Matter* **20**, 064201 (2008).
- ²⁴ J. L. Lyons, A. Janotti, and C. G. V. de Walle, *Appl. Phys. Lett.* **95**, 252105 (2009).
- ²⁵ C. G. Van de Walle and A. Janotti, *Phys. Status Solidi B* **248**, 19 (2011).
- ²⁶ A. Alkauskas, P. Broqvist, and A. Pasquarello, *Phys. Status Solidi B* **248**, 775 (2011).

- ²⁷ J. L. Lyons, A. Janotti, and C. G. Van de Walle, *Phys. Rev. Lett.* **108**, 156403 (2012).
- ²⁸ G. Kresse and J. Hafner, *J. Phys.: Condens. Matter* **6**, 8245 (1994).
- ²⁹ G. Kresse and D. Joubert, *Phys. Rev. B* **59**, 1758 (1999).
- ³⁰ P. E. Blöchl, *Phys. Rev. B* **50**, 17953 (1994).
- ³¹ A. V. Krukau, O. A. Vydrov, A. F. Izmaylov, and G. E. Scuseria, *J. Chem. Phys.* **125**, 224106 (2006).
- ³² J. P. Perdew, K. Burke, and M. Ernzerhof, *Phys. Rev. Lett.* **77**, 3865 (1996).
- ³³ S. Grimme, *J. Comput. Chem.* **27**, 1787 (2006).
- ³⁴ T. Bučko, J. Hafner, S. Lebègue, and J. Ángyán, *J. Phys. Chem. A* **114**, 11814 (2010).
- ³⁵ L. Liu, Y. P. Feng, and Z. X. Shen, *Phys. Rev. B* **68**, 104102 (2003).
- ³⁶ N. Marom, J. Bernstein, J. Garel, A. Tkatchenko, E. Joselevich, L. Kronik, and O. Hod, *Phys. Rev. Lett.* **105**, 046801 (2010).
- ³⁷ R. S. Pease, *Acta Crystallographica* **5**, 356 (1952).
- ³⁸ H. J. Monkhorst and J. D. Pack, *Phys. Rev. B* **13**, 5188 (1976).
- ³⁹ S. B. Zhang and J. E. Northrup, *Phys. Rev. Lett.* **67**, 2339 (1991).
- ⁴⁰ D. B. Laks, C. G. Van de Walle, G. F. Neumark, P. E. Blöchl, and S. T. Pantelides, *Phys. Rev. B* **45**, 10965 (1992).
- ⁴¹ C. G. V. de Walle and J. Neugebauer, *J. Appl. Phys.* **95**, 3851 (2004).
- ⁴² X. Blase, A. Rubio, S. G. Louie, and M. L. Cohen, *Phys. Rev. B* **51**, 6868 (1995).
- ⁴³ G. Cappellini, G. Satta, M. Palummo, and G. Onida, *Phys. Rev. B* **64**, 035104 (2001).
- ⁴⁴ B. Arnaud, S. Lebègue, P. Rabiller, and M. Alouani, *Phys. Rev. Lett.* **96**, 026402 (2006).
- ⁴⁵ G. Henkelman, A. Arnaldsson, and H. Jónsson, *Comput. Mater. Sci.* **36**, 354 (2006).
- ⁴⁶ V. Wang, H. Mizuseki, H. He, G. Chen, S. Zhang, and Y. Kawazoe, *Comput. Mater. Sci.* **55**, 180 (2012).